ROYAL SOCIETY
OF CHEMISTRY

Check for updates

Mechanochemical preparation of donor/acceptor adducts based on coronene and silver(I) pyrazolate metallacycles†

Lorenzo Luciani, Nicola Sargentoni, Claudio Magini and Rossana Galassi [ID] *

The preparation of materials having optical properties is a fertile area of research because of their application in OLEDs, sensors, and semiconducting materials science field. Moreover, considering environmental concerns, there is an increasing need in the scientific community to enhance the preparative methods using eco-friendly approaches. In this work, the mechanochemical liquid assisted grinding (LAG) method is applied for the syntheses of hybrid organometallic/organic materials made of π−acidic silver(I) or copper(I) metallacycles, with bridging ligands such as 3,5-bis(trifluoromethyl) pyrazolate or 3,5-dinitro-pyrazolate, and coronene, a highly symmetric polycyclic aromatic molecule (PAH). The LAG method was monitored by FT-IR spectroscopy and SEM; the former was applied to study the slight structural modification upon interactions, and the latter was used to depict the changes in the solid surface morphology upon CH_2Cl_2-assisted grinding. On the other hand, the dissolution of the materials reversibly yields the starting compounds. The stacked materials were characterized by elemental and TGA analyses, and photoluminescence (PL), and IR spectroscopies. The PL study highlights the room temperature quenching of the coronene emissions at 505 nm, indicating the occurrence of dispersive electrostatic interactions. Interestingly, the solid-state UV-Vis study allowed the calculations of direct (2.27 eV) and indirect (2.78 eV) band gaps for the D/A adduct {[3,5-$(CF_3)_2$pz]Ag}$_3$@coronene, **1**, with values featuring the materials in the semiconductor band gap range, useful for application in OFETs or OPVs.
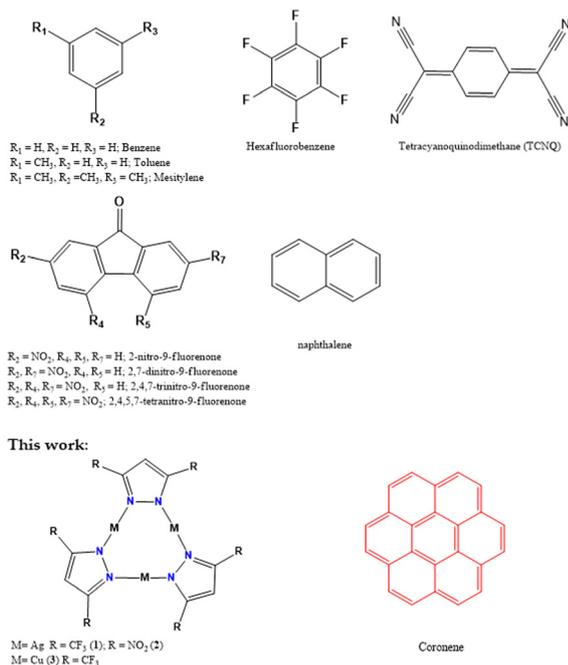
Introduction

In the last few years, the design of alternative semiconducting materials has received much attention due to their potential for application in optoelectronic devices, like organic light-emitting diodes (OLEDs), organic photovoltaic cells (OPVs) and organic field-effect transistors (OFETs). Meanwhile, the superior performance as emitting materials, consisting of near unit quantum yields and high tunability of the emission colours, in addition to thermal and air stability of Au(I), Ag(I), and Cu(I) cyclic trinuclear metallacycles, CTCs, made them popular in the optoelectronics field.[1,2] CTCs are cyclic compounds made of metals in the +1 oxidation state, generally bridged by mono-negative bi-hapto azolates. The donor–acceptor ability of CTCs depends on the metal, the type of azole, and the substituents on it.[3] In addition, in the solid state, CTCs possess the ability to form supramolecular, extended structures

via cooperative binding interactions, ranging from dispersive to closed shell attractive forces. Integrated experimental/computational studies support that donor–acceptor (D/A) systems based on these CTCs are stabilized by π–π interactions and electrostatic and dispersive forces.[4] The formation of D/A systems based on Au(I), Ag(I), and Cu(I) CTCs gives rise to a variety of photophysical phenomena, for example, thermochromic luminescence,[5–7] quenching in solution[8] and/or light emission shifts by exposing to small molecule vapours,[5,8,9] and selected light emission shifts.[10–13] Noteworthy, a Au(I) CTC, with a carbeniate as the bridging ligand, acts as a molecular nanowire exhibiting a p-type field effect when it is applied in a transistor;[14] in addition, studies on the hole transport of this CTC, upon doping within a poly(9-vinyl carbazole) host, detail that a high increase in current density from $\sim$1 to $\sim$1000 mA cm^{-2} was observed. The formation of D/A systems using CTCs, depending on their π–acid or π–basic behaviour, can be achieved by interaction with small organic molecules,[8] with Lewis acids or bases,[15–17] by the stacked combination of CTCs with complementary π–acidic/π–basic properties,[4,18] and, finally, by clustering with soft metal cations such as (Cu(I), Ag(I), Tl(I)).[16,18,19] Remarkably, CTCs stack with small aromatic

School of Science and Technology, Chemistry Division, University of Camerino, Camerino, I-62032, Italy. E-mail: rossana.galassi@unicam.it

† Electronic supplementary information (ESI) available. See DOI: https://doi.org/10.1039/d3nj02614k

This journal is © The Royal Society of Chemistry and the Centre National de la Recherche Scientifique 2023

Scheme 1 Top: Examples of aromatic molecular structures applied in forming D/A adducts with CTCs and reported in the literature. Bottom: molecular structures of the CTCs herein considered and of coronene.

moieties, like benzene,[7] toluene,[7] mesitylene,[10] TCNQ and hexafluorobenzene (TetraCyaNoQuinodimethane),[8] and extended arene systems like naphthalene[6] and nitrofluorene[9] (see Scheme 1) to form isolated binary D/A or extended supramolecular structures of the type $\{ADAD\}_n$, $\{ADDA\}_n$ (where A = acceptor, D = donor, with n going from 2 to infinite). The formation of extended structures has been extensively observed in the solid state, and the persistence of oligomeric structures of D/A adducts was detected in solution by PGSE determination.[20] Among aromatic organic molecules, polycyclic aromatic hydrocarbons (PAH) are a class of planar π-conjugated organic molecules, comprising two or more fused benzene rings that are known to be efficient organic semiconductors,[21,22] with high charge-carrier mobility and reduced band gap, enabling them as excellent materials for application in OFETs.[23–25] Other purely organic, organometallic, or semiconducting polymers with extended π-conjugated systems are a staple for present and future developments of OLED[26] and OPV[27] devices. Among other PAHs, coronene has attracted attention for many peculiar properties: it is a blue emitter substance;[28] it forms supramolecular architecture by π–π interactions and/or van der Waals interactions;[29] and it is a versatile constituent of semiconducting materials.[30]

In the last few decades, the arising climatic crisis has pushed chemists to use cleaner chemical processes that involve the use of smaller amounts of harmful solvents and restricted energy consumption in addition to shorter reaction times. In this context, mechanochemistry represents a powerful tool for synthetic chemists because it contemplates the absence or the use of limited solvent quantities. It is noteworthy that mechanochemistry usually allows more facile scalability, from milligram scales to industrial productions, compared to classical solvent-mediated approaches. In the last few years, mechanochemistry has been successfully applied for the synthesis of organic compounds, main group inorganic salts, inorganic or organometallic block-d complexes, coordination polymers and MOFs, nanocomposites, and nanoparticles with applications in many fields of medicinal chemistry or energy storage and production.[31,32] By considering what is quoted above, the herein work is focused on the preparation of hybrid D/A materials made of two different π–acid CTCs and coronene (see Scheme 1) to prepare semiconductive/photo-emissive materials, potentially applicable in large-scale production. The plan is based on the assumption that D/A adducts generally feature low activation energy barriers and by considering the potential of PAHs in sensitizing group 11th CTCs; herein we present both the solvent-mediated and unprecedented mechanochemical preparation of D/A adducts made of electron-rich coronene and π–acid silver(I) or copper(I) pyrazolate CTCs, aiming to find a green path to synthesize these hybrid materials.

Results and discussion

Solvent-mediated preparation

The reactions proceed by mixing CH_2Cl_2 or THF solutions of the Cu(I) or Ag(I) CTCs (with the bridging ligand 3,5-dinitropyrazolyl[15] or 3,5-bis(trifluoromethyl)pyrazolyl)[33] with coronene in a 1:1 molar ratio to obtain the adducts **1–3** by crystallization (Scheme 2). In general, upon mixing the CTCs and the organic molecule, fast precipitation of pale yellowish solids was observed, particularly for the adduct $\{[3,5-(NO_2)_2$-pz]Ag\}_3$@coronene, **2**, resulting in the least soluble adduct. Crystallization of **1** and **3** was performed by dissolving the microcrystalline solids in toluene and adding a few drops of hexane, yielding very small needle-shaped crystals of **1**. Crystals of **1** are pale yellow, while those of **2** and the microcrystalline powder of **3** are yellow. The elemental analysis matches the 1:1 molar ratio between the coronene and the corresponding starting CTC. In the ^1H NMR spectra of **1–3**, only two resonances were recorded, attributable to the magnetically equivalent terminal C–H hydrogen atoms of the coronene and the C_4–H of the pyrazole ligands in the CTCs, with only the latter
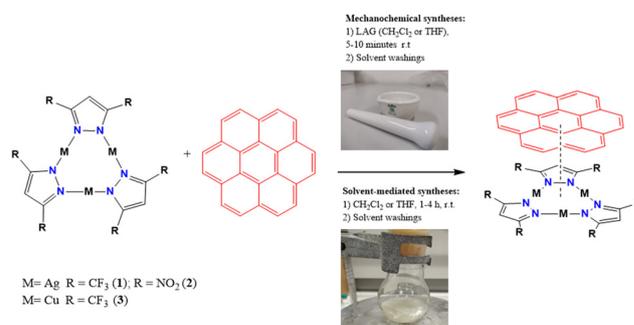
Scheme 2 Procedures performed for the preparation of adducts **1–3**.

slightly shifted to low frequencies (from 0.03 ppm for **3** to 0.16 ppm for **2**) with respect to those of pristine Cu(ɪ)/Ag(ɪ) CTCs (see Table S1 and Fig. S1–S3 in ESI†); the integration of these two peaks matches with the 1:1 molar ratio for all the adducts. The mild shifts might be imputed to the fact that the dissolution of the adducts competes with a dissociative equilibrium reaction restoring the starting materials. A similar behaviour, both in dissociation and in ^{1}H NMR chemical shift variations, was already observed for analogous D/A hybrid adducts,[15,34–36] as, for example, the one composed of $\{[3,5\text{-}(CF_3)_2pz]Cu\}_3$ and DBTTF or TTF (DiBenzoTetraThioFulvalene or TetraThioFulvalene), for which D/A binding energies of the order of magnitude of an ionic bond were calculated.[34] Equilibria in solutions for D/A systems were already studied[35] for adducts made of donor Au(ɪ) CTCs, for example $\{[\mu\text{-}C,N\text{-imidazolyl-2yl}]Au\}_3$, and organic π-conjugated systems as acceptors; association constants were found to range in the 10^2–10^4 M order of magnitude in dichloromethane.[35] Higher association constants, in the 10^4–10^7 M range, were obtained for D/A systems composed of π–basic Au(ɪ) CTCs and π–acid Cu(ɪ)/Ag(ɪ) CTCs, where the probable occurrence of closed shell d^{10}–d^{10} bonding reinforces the binding energy of the D/A systems.[36]

Concerning the IR spectroscopy characterization of adducts **1–3**, mild shifts ranging from a few units to tens of cm^{-1} were observed. Table S2 (ESI†) reports the main solid-state IR data recorded for the adducts **1–3**, compared with those of the starting compounds. In particular, in the case of adducts $\{[3,5\text{-}(CF_3)_2pz]Ag\}_3$@coronene, **1**, and $\{[3,5\text{-}(CF_3)_2pz]Cu\}_3$@coronene, **3**, the characteristic peaks of the starting CTCs were redshifted, when compared to those of the starting CTCs. For example, the C_4–H stretching of **1** and **3** was redshifted by 4 and 14 cm^{-1}, respectively. In turn, the characteristic peaks of the coronene in **1** and **3** adducts were blue-shifted by about 3 cm^{-1} with respect to the pristine coronene. The reversed trend in the shifts has been found for $\{[3,5\text{-}(NO_2)_2pz]Ag\}_3$@coronene, **2**, and most of the peaks are blue-shifted with respect to both starting $\{[3,5\text{-}(NO_2)_2pz]Ag\}_3$ and coronene compounds. In this regard, in a previous work,[15] it was defined that despite the structural analogy of the CTCs and the similar electron-withdrawing features of the substituents in the 3,5 position of the pyrazole, between the $\{[3,5\text{-}(NO_2)_2pz]Ag\}_3$ and $\{[3,5\text{-}(CF_3)_2pz]Ag\}_3$, a significantly less polarizable electrostatic potential and higher argentophilic characteristics were modelized for the latter, defining a boundary line in the electronic acceptor/donor features of these CTCs.[15]

Mechanochemical preparation

Aiming to explore greener techniques, concomitantly to the solvent-mediated preparations, several mechanochemical methods were attempted to prepare adducts **1–3**. The successful procedure consisted of 10–30 minutes of liquid assisted mechanical grinding (LAG) (in CH_2Cl_2 or THF) of a 1:1 molar ratio of the reactants, Ag(ɪ) or Cu(ɪ) CTCs and coronene, in a common ceramic mortar. The reactions were monitored by acquiring the IR spectra of the powder mixtures and comparing them with the IR spectra of the adducts **1–3** obtained by

solvent-mediated synthesis (see Fig. S4a–c, ESI†). After washing with the minimum quantity of solvent, the adducts **1–3** were isolated in fairly good yields (65–76%). The IR, ^{1}H NMR spectra, and the TGA plots were superimposable allowing us to establish the success of the preparation (see materials and methods). The completely solventless mechanochemical grinding approach, as well as the ball mill procedures, even prolonged for hours, yielded low conversion ratios to the final adducts **1–3**, confirming the need of adding few solvent drops to get the final adducts in good yields.

Scanning electron microscopy (SEM)

The SEM analyses were performed to compare the samples' morphology and topography obtained by the two different preparative approaches: solvent-assisted preparation and LAG mechanochemical preparation. The SEM images were recorded on the starting materials ground with and without a few drops of solvent, and the images were compared to the solids of the final adduct **1** obtained by the two methods. All the scans were acquired after solventless grinding (SG) and dichloromethane-assisted grinding (LAG) (grinding time: 5 min each). The energy dispersive X-ray (EDX) analysis revealed the presence of O, Si, and Al impurities due to the ceramics used in the grinding processes. The SEM images of the compound $\{[3,5\text{-}(CF_3)_2pz]Ag\}_3$ highlighted that contrary to what was observed with the SG, the treatment with CH_2Cl_2 results in loss of crystallinity and agglomeration of the particles (Fig. 1).

In Fig. 2, the SEM images of solventless grinding of coronene showed nano tubular-like morphology (Fig. 2, left), which was largely maintained after grinding with dichloromethane (Fig. 2, right); the LAG in coronene causes an expansion of the nanotubular structures with diameters increasing
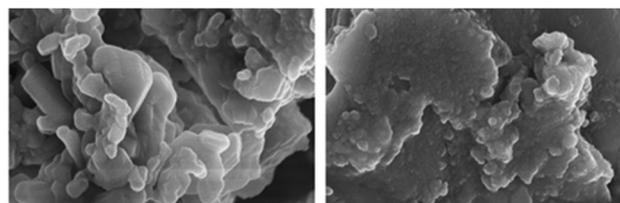

Fig. 1 150 KX SEM image of $\{[\mu\text{-}3,5\text{-}(CF_3)_2pz]Ag\}_3$; left: solventless ground $\{[\mu\text{-}3,5\text{-}(CF_3)_2pz]Ag\}_3$; right: dichloromethane LGA ground $\{[\mu\text{-}3,5\text{-}(CF_3)_2pz]Ag\}_3$.
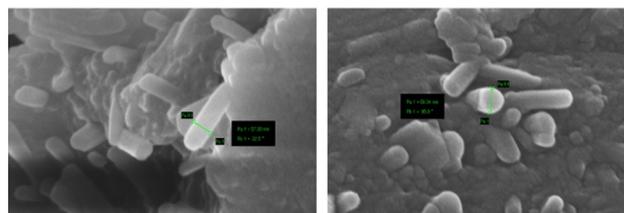

Fig. 2 300 KX SEM images of coronene after solventless grinding (left), and after grinding with CH_2Cl_2 (right). The green segments depict the tubular size measurements.
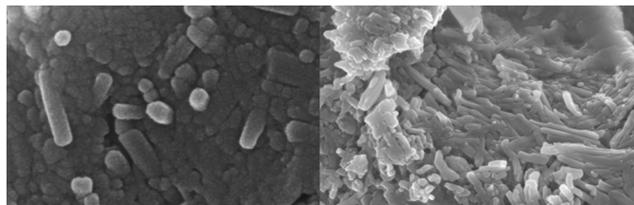
Fig. 3 SEM images recorded for the preparation of adduct {[μ-3,5-(CF$_3$)$_2$pz]Ag}$_3$/coronene, **1**, with different mechanochemical methods; left: after solventless grinding, diameters of the tubular structures are mostly unchanged: 50.34 nm, 45.70 nm (300 K X); right: after dichloromethane LAG, larger diameters of the tubular structures resulted: 167.6 nm, 175.3 nm (right, 50 K X) with an increase of the overall crystallinity.

from 40–60 nm to 65–80 nm (from 57.30 nm to 68.04 nm in Fig. 2), and a partial loss of crystallinity.

The comparison of the SEM images recorded for the {[μ-3,5-(CF$_3$)$_2$pz]Ag}$_3$/coronene mixture after solventless or LAG grinding highlighted notable differences. In detail, after solventless grinding, the diameters of the nanotubular structures were almost comparable to those of pristine coronene with a tubular diameter ranging from *ca.* 45 to 50 nm (Fig. 3, left). Conversely, after dichloromethane LAG grinding, the diameters of the nanotubular structures largely increased, reaching values ranging from 167.6 nm to 175.3 nm (Fig. 3, right). These observations are consistent with the formation of large co-crystals of the adduct by an expansion of the crystals of the adduct.[37,38]

Concurrently, the EDX analysis of the {[3,5-(CF$_3$)$_2$pz]Ag}$_3$/coronene samples, acquired on samples obtained by the solventless or LAG method, confirmed the previous observation consisting of a larger sample homogeneity of the composition in the sample obtained by the LAG method than that obtained with the SG method (Tables S3 and S4, ESI†). In addition, the surface morphologies and topologies were much more homogeneous in the case of the former sample (Fig. 4 and 5).

Thus, the LAG process favors the rapid and complete conversion of the reactants to adduct **1** (10 minutes), which could not be
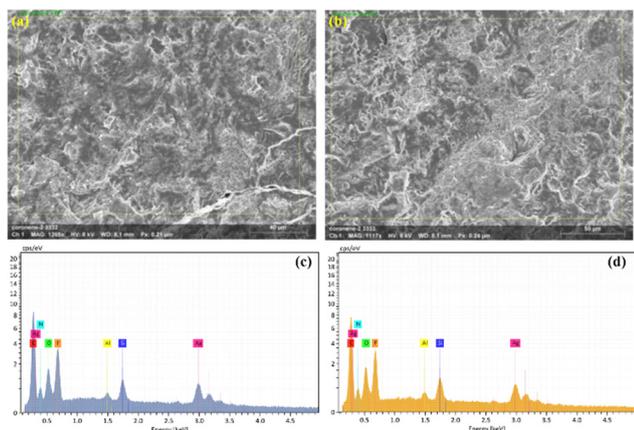

Fig. 4 SEM images of the adduct {[μ-3,5-(CF$_3$)$_2$pz]Ag}$_3$/coronene obtained by the mechanochemical grinding; (a) scan of the spot 1; (b) scan of the spot 2 at different resolution; (c) EDX analysis of the spot 1; (d) EDX analysis of the surface of the spot 2. Si and O are due to the mortar.
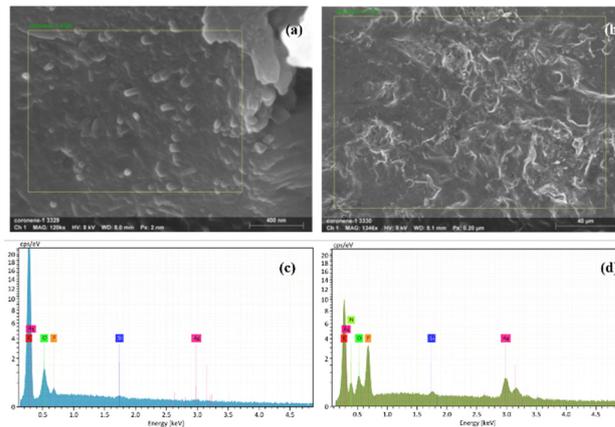

Fig. 5 SEM images of the adduct formed by {[μ-3,5-(CF$_3$)$_2$pz]Ag}$_3$/coronene after dichloromethane LGA; (a) scan of spot 3; (b) scan of spot 4; (c) EDX analysis of spot 3; (d) EDX analysis of spot 4. Si, Al, and O are due to the mortar.

obtained even after prolonged solventless grinding (1 hour). Moreover, adding a small aliquot of a solvent in which the starting compounds are at least partially soluble, facilitating the formation of D/A co-crystals at the interface, is a fundamental step to obtain fast and complete reactions through mechanochemistry.[37,39]

TGA Analyses of the adducts 1–3

Since thermal stability is fundamental in applying molecular substances as materials, thermogravimetric analysis (TGA) on the solid microcrystalline samples of **1–3** was performed. The adducts **1–3** display thermal stabilities comparable to that of coronene, featuring weak intermolecular bonding in D/A co-crystals. However, **1–2** display the main weight loss at around 400 °C (Fig. 6(a) and (b)) while **3** displays stepwise losses starting at about 200 °C till 260 °C concluding at 380 °C (Fig. 6(c)). In all cases, the weight losses involved the organic moieties of the adducts, with a weight residue that roughly corresponds to metallic Ag, in the case of {[3,5-(NO$_2$)$_2$pz]Ag}$_3$@coronene, **2**, and AgF and CuF$_2$ for **1** and for **3**, respectively. Details on the weight losses are reported in Fig. S5 (ESI†).
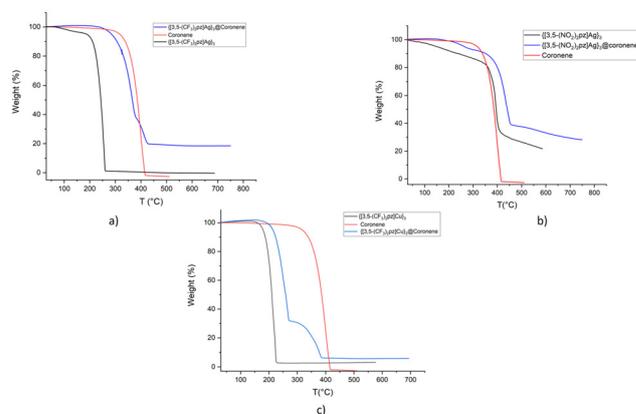

Fig. 6 TGA plots of the adducts **1** (a), **2** (b), and **3** (c) in comparison to those of the starting compounds.

Solid-state luminescence studies

The solid-state photoluminescence (PL) of D/A adducts **1–3** at room temperature was evaluated and compared to the PL of the starting compounds (see Fig. 7 and Fig. S6–S9, ESI†). The PL studies were conducted only in the solid state, as at the concentrations suitable for the acquisition of PL spectra, no spectral changes were detected (Fig. S10, ESI†). While {[3,5-$(CF_3)_2$pz]Cu}$_3$ and coronene are strongly luminescent with red (625 nm) and green (505 nm) emissions, respectively, {[3,5-$(NO_2)_2$pz]Ag}$_3$ and {[3,5-$(CF_3)_2$pz]Ag}$_3$ are not emissive at room temperature. Fig. 7 shows the normalized luminescence spectra of the co-crystals of **3** upon excitation at 320 nm in comparison with those of coronene and of the starting {[3,5-$(CF_3)_2$pz]Cu}$_3$; the emissions of **3** are slightly blue-shifted with respect to those of coronene and {[3,5-$(CF_3)_2$pz]Cu}$_3$, with shifts from 505 nm to 482 nm in **3** and from 625 nm to 620 nm in **3**, respectively. Similar behaviours were also detected for adducts **1** and **2** (Fig. S6, ESI†). The formation of the adducts **1–3** causes a decrease of the fluorescence intensity of the coronene centred emissions and the eventual quenching of that of CTC. Metallaromatic and organic aromatic molecules can make stable adducts in the solid state mainly *via* dispersive forces, attractive orbital interactions, electrostatic forces, and hydrogen bonding.[40] Due to the lack of hydrogen donor/acceptor sites in the considered systems and considering the π–acidic and π–basic nature of the CTCs and coronene, respectively, it is expected that the solid-state adducts are stabilized mainly by electrostatic interactions and by dispersive forces. Therefore, the observed total quenching might be due to Aggregation-Caused-Quenching (ACQ)[41,42] consistent with the π–π interaction of the CTCs and the coronene moieties.[43] However, the findings of this study are in contrast with those reported in a previous study of arene/CTCs adducts, where the persistence or the sensitization of bright emissions in the visible range was observed.[6]
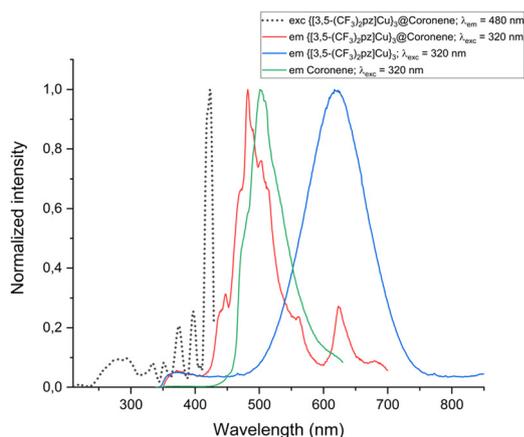

Fig. 8 Normalized solid state UV-Vis absorption spectra of {[3,5-$(CF_3)_2$pz]Ag}$_3$@coronene, **1** (red curve), of coronene (black curve) and of {[3,5-$(CF_3)_2$pz]Ag}$_3$ (blue curve).

Solid-state UV-Visible spectroscopy on adduct {[3,5-$(CF_3)_2$pz]Ag}$_3$@coronene, 1

The solid state UV-Vis spectrum of {[3,5-$(CF_3)_2$pz]Ag}$_3$@coronene, **1**, was acquired and compared to those of the starting compounds (Fig. 8). Adduct **1** showed absorption bands in the 250–480 nm range, mainly consisting of shifted bands due to {[3,5-$(CF_3)_2$pz]Ag}$_3$ and coronene absorptions, and a low-intensity band centered around 560 nm, which might be attributed to a charge transfer due to the D/A system.[29,44] It is noteworthy that a weak emission at 560 nm (2.21 eV) is also observed upon excitation at 320 nm (Fig. 8).

The direct and indirect energy band gaps of {[3,5-$(CF_3)_2$pz]Ag}$_3$@coronene, **1**, were calculated to be 2.78 eV and 2.27 eV, respectively (Fig. 9).

The energy band gap of **1** is smaller than those calculated for the starting Ag(I) CTC and for coronene, displaying band gaps of 3.74 eV, 3.13 eV (see Fig. S11, ESI†), and 3.22, 2.89 eV,[44] respectively, (see Fig. S12, ESI†) for direct and indirect band gaps. Therefore, in addition to the quenching of the photo-emissions a lowering of the energy band gap was attained, likely due to a new electronic distribution in the MOs of the adduct. The calculated band gaps for **1** pose this material in the range of typical organic π-conjugated semiconductors like rubrene, pentacene, oligothiophenes, oligo-phenylamines, or

Fig. 7 Normalized solid state excitation/photoemission spectra of the adduct {[3,5-$(CF_3)_2$pz]Cu}$_3$@coronene, **3**, on comparison with those of coronene (black curve) and of {[3,5-$(CF_3)_2$pz]Cu}$_3$ (red curve), upon excitation at 320 nm.
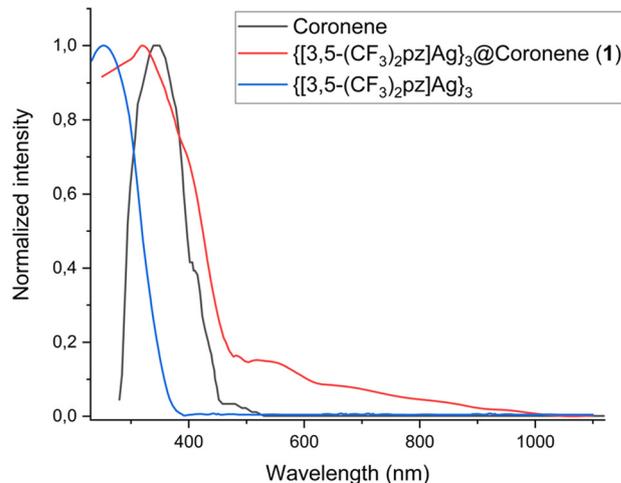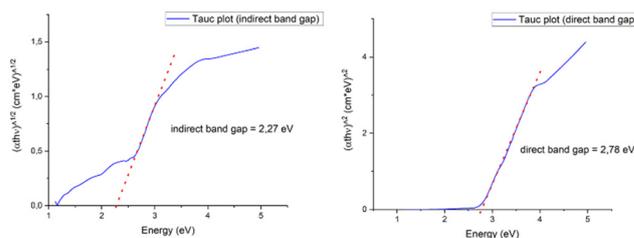

Fig. 9 Solid state Tauc plots of {[3,5-$(CF_3)_2$pz]Ag}$_3$@coronene, **1**, with indirect (left) and direct (left) band gap calculations.

the well-known Al and Ga complexes of hydroxyquinoline, exhibiting band gaps ranging between 1.8 eV and 3 eV; hence, adduct **1** falls in the band gap range of a semiconductor.[29,45]

Experimental section

Materials and methods for the preparation

All the air-sensitive synthetic steps were performed under an inert atmosphere using the Standard Schlenk technique. Deuterated solvents were purchased from Merck and used as received. 3,5-Bis(trifluoromethyl)pyrazole and coronene were purchased from Merck and used without further purification. $\{[Cu(\mu\text{-}3,5\text{-}(CF_3)_2pz)]\}_3$, $\{[Ag(\mu\text{-}3,5\text{-}(CF_3)_2pz)]\}_3$ and $\{[Ag(\mu\text{-}3,5\text{-}(NO_2)_2pz)]\}_3$ were synthesized as described in the literature.[15,33] Mechanochemical syntheses were performed by grinding the microcrystalline powders in a common ceramic mortar without solvents or in the presence of a few drops of CH_2Cl_2 or THF until the complete conversion of the reactant toward the products occurred, as checked by FT-IR analysis.

Physical measurements

The mid-infrared (IR) spectra were collected on a Thermo-Scientific Nicolet-6700 Fourier transform-infrared (FTIR) spectrophotometer with a smart orbit diamond attenuated total reflectance (ATR) accessory, by firmly pressing the neat sample onto the diamond plate of the ATR accessory. The IR spectra were recorded from 4000–700 cm^{-1} (Mid-IR range) and 700–100 cm^{-1} (Far-IR) under an N_2 atmosphere. ^{1}H-NMR spectra were acquired using a 500 Bruker Ascend (500 MHz for ^{1}H). The chemical shifts of the ^{1}H-NMR spectra were expressed in ppm and related to Me$_4$Si. The annotations used are s = singlet and br = broad. Solid-state UV-Vis absorbance spectra were acquired with a PerkinElmer Lambda 35 UV/VIS spectrophotometer equipped with a lab-sphere RSA-PE-20 reflectance spectroscopy accessory. Blanks were acquired using labsphere certified reflectance standards and were subtracted from the signals of the samples. Determination of direct and indirect band gaps was extrapolated by absorbance data, and the mathematical elaborations were made according to Tauc plot graphical methods, considering a thickness of the film of 0.2 cm.[46] Crystalline samples were prepared by grinding and placing an adequate amount of fine powder on the sample holder, to obtain a layer measured in *ca.* 0.2 cm. Elemental analyses (C, H, N, and S) were performed in-house with a Fisons Instrument 1108 CHNS-O elemental analyzer. An SMP3 Stuart Scientific Instrument and an Electrothermal Mel-Temp melting point device were used to determine the melting point. Thermogravimetric analysis (TGA) was performed under a N_2 flow (10 mL min^{-1}) with a PerkinElmer Simultaneous Thermal Analyzer STA 600, by setting a heating ramp from 30.00 °C to 700.00 °C (10 °C min^{-1}). Solid-state photoluminescence spectra were acquired using a Horiba FluoroMax spectrofluorometer by placing the microcrystalline powder on a solid sample holder. The scanning electron microscopy (SEM) and energy dispersive X-ray (EDX) analyses were performed using a Zeiss Sigma 300

FE-SEM equipped with a Bruker QUANTAX EDX detector. The analyses were performed by detecting secondary electrons, with image acquisitions with the following magnification values: 50 K X, 150 K X, and 300 K X.

Preparation of $\{[3,5\text{-}(CF_3)_2pz]Ag\}_3$@coronene, 1

Solvent-mediated preparation. Solid coronene was dissolved in 3 mL of CH_2Cl_2 (10.2 mg; 0.034 mmol) and added dropwise to a 3 mL dichloromethane solution of $\{[3,5\text{-}(CF_3)_2pz]Ag\}_3$ (31.2 mg; 0.034 mmol). After a few minutes, a pale-yellow precipitate was formed, and the suspension was stirred for 3 h at room temperature. The solution was centrifuged and washed with CH_2Cl_2 (3 mL × 3 times), and the pale yellowish solid was collected. The solid was crystallized by slow evaporation from a solution of toluene layered with hexane. After a few days, white needles precipitated. Yield of 80% MM = 1233.15 g mol^{-1}.

Mechanochemical preparation. Solid $\{[3,5\text{-}(CF_3)_2pz]Ag\}_3$ (30 mg, 0.032 mmol) and coronene (9.6 mg, 0.032 mmol) were mixed in a mortar and ground together for 10 minutes with few drops of CH_2Cl_2 to obtain a fine powder in a mortar. The solid was recovered in THF, filtered with a PTFE filter (0.45 μm), and dried at reduced pressure. The pale-yellow solid was washed with hexane (1 mL × 3 times) and the precipitate was dried at reduced pressure. Yield: 75%. MM = 1233.15 g mol^{-1}.

The following characterization studies were performed on the sample obtained by the mechanochemical method.

MIR (cm^{-1}): 3149 (w), 3063 (w), 3029 (w), 1618 (w), 1610 (w), 1545 (w), 1502 (w), 1454 (w), 1357(w), 1315 (w),1260 (s), 1224 (m), 1162 (sh, m), 1129 (s), 1091 (sh, w), 1024 (s), 987 (w), 861 (s), 814 (sh, w), 800 (m), 768 (w), 756 (m), 735 (w), 710 (w).

FIR (cm^{-1}): 609 (w), 579 (w), 548 (s), 483 (m), 425 (w), 378 (m), 360 (w), 242 (s), 219 (sh, m), 206 (sh, w), 192 (sh, m), 182 (s), 168 (sh, m), 156 (sh, m), 150 (m), 145 (sh, m), 134 (m), 121 (s), 110 (sh, m), 102 (s).

^{1}H NMR (DMSO, δ): 9.10 (s, 12H); 7.10 (s, 3H).

^{1}H NMR (THF, δ): 9.00 (s, 12H); 7.35 (s, 3H).

Elemental analysis calculated for $C_{39}H_{15}Ag_3F_{18}N_6$: C 37.99; H 1.23; N 6.82; found: C 38.21; H 1.40; N 6.31.

TGA analysis (1.1134 mg): first weight loss from 223 to 379 °C (−61.59%) corresponds to the loss of 3 molecules of coronene, 1 molecule of the silver CTC, and 3 molecules of the starting ligand (*via* silver CTC decomposition). The second weight loss from 379 °C to 428 °C (−18.57%) corresponds to the loss of a molecule of silver CTC; and the third weight loss occurs at 428 °C to 364 °C (−1.5%). The residual weight of 18.34% roughly corresponds to 1AgF + 1Ag (metallic silver) residue.

Preparation of $\{[3,5\text{-}(NO_2)_2pz]Ag\}_3$@coronene, 2

Solvent-mediated preparation. Solid coronene was dissolved in 2 mL of THF (3.4 mg; 0.0113 mmol) and added dropwise to a 4 mL THF solution of $\{[3,5\text{-}(NO_2)_2pz]Ag\}_3$ (9 mg; 0.0113 mmol). A ready precipitation of a yellow solid was observed. After 1 hour, the yellow precipitate was centrifuged and washed with THF (3 mL × 2 times), dichloromethane (3 mL × 2 times), and dried under a vacuum. The solid is insoluble in most organic

solvents, and only slightly soluble in DMSO. Yield of 84%. MM = 1095.15 g mol^{-1}.

Mechanochemical preparation. $\{[3,5\text{-}(NO_2)_2pz]Ag\}_3$ (26 mg, 0.0327·mmol) and coronene (9.82 mg, 0.0327·mmol) were ground together in a common ceramic mortar with THF, for 10 minutes. The resulting powder was recovered and washed with THF (2 × 1 mL) and CH_2Cl_2 (2 × 1 mL) and the solid was dried at reduced pressure. Yield: 76%. MM = 1095.15 g mol^{-1}.

The following characterization studies were performed on the sample obtained by the mechanochemical method.

MIR (cm^{-1}): 3160 (w), 3063 (w broad), 2853 (w), 2761 (w), 1608 (w), 1552 (m), 1497 (s), 1461 (sh,w), 1365 (m), 1331 (s), 1314 (sh, m), 1301 (sh, w), 1201 (w), 1158 (w), 1137 (w), 1074 (w), 1048 (m), 1014 (w), 870 (m), 835 (s), 815 (sh, m), 768 (w), 741 (m).

FIR (cm^{-1}): 591 (w), 552 (m), 378 (w), 368 (w), 313 (w), 303 (sh, w), 291 (w), 244 (w), 231 (sh, w), 221 (w), 206 (sh, w), 195 (m), 191 (m), 181 (m), 167 (w), 152 (s), 142 (s), 133 (m), 115 (m), 109 (w), 102.33 (s).

^{1}H NMR (DMSO, δ): 9.10 (s, 12H); 7.40 (s, 3H).

Elemental analysis for $C_{35}H_{19}Ag_3N_{12}O_{12}Cl_4$ (1 adduct 1 : 1+2 molecules of CH_2Cl_2): C 33.23; H 1.58; N 13.29; found: C 33.86; H 1.67; N 12.22.

TGA analysis: (1.646 mg) first weight loss from 30 °C to 281 °C (−7%, loss of CH_2Cl_2); second weight loss from 281 °C to 453 °C (−53, 16%); and third weight loss (−11, 51%). The residual weight (28.33%) corresponds to 3 moles of metallic silver.

Preparation of $\{[3,5\text{-}(CF_3)_2pz]Cu\}_3$@coronene, 3

Solvent-mediated preparation. $\{[3,5\text{-}(CF_3)_2pz]Cu\}_3$ (29 mg; 0.0366 mmol) was added to a solution of coronene (11 mg; 0.0366 mmol) dissolved in 8 mL of CH_2Cl_2; ready precipitation of a light-yellow solid was observed. After 4 hours, the yellow precipitate was centrifuged and dried under reduced pressure. The solid was washed with hexane (3 × 2 mL) and dried at reduced pressure. Yield of 70%. MM = 1100.19 g mol^{-1}.

Mechanochemical preparation. $\{[3,5\text{-}(CF_3)_2pz]Cu\}_3$ (30 mg, 0.0375 mmol) and coronene (11.2 mg, 0.0375 mmol) were ground together in a common ceramic mortar, for 10 minutes, with few drops of CH_2Cl_2. Then, the resulting powder was dissolved in CH_2Cl_2, filtered on a PFTE filter (0.45 μm), and dried at reduced pressure. The solid was washed with hexane (3 times with 1 mL) and then dried at reduced pressure. Yield: 65%. MM = 1100.19 g mol^{-1}.

The following characterization studies were performed on the sample obtained by the mechanochemical method.

MIR (cm^{-1}): 3149 (w), 3060 (w), 3026 (w), 2964 (w), 2912 (w), 1618 (w), 1610 (w), 1552 (w), 1539 (w), 1506 (w), 1457 (w), 1451 (w), 1416 (w) 1365 (w), 1315 (m), 1258 (m), 1224 (m), 1183 (sh, m), 1158 (sh, s), 1130 (s), 1120 (sh, s), 1034 (s), 991 (m), 968 (sh, m), 862 (m), 823 (m), 819 (m), 769 (w), 759 (m), 735 (m), 715 (w).

FIR (cm^{-1}): 693 (w), 686 (sh, w), 677 (sh, w), 661 (w), 646 (w), 638 (w), 624 (w), 613 (w), 583 (w), 566 (w), 550 (s), 497 (s), 467 (m), 455 (w), 441 (w), 419 (w), 397 (w), 378 (m), 360 (w), 342 (w), 332 (w), 313 (w), 301 (w), 287 (w), 268 (m), 258 (m), 246 (w), 225 (s), 211 (sh, m), 188 (w), 181 (w), 174 (w), 160 (w), 152 (m), 141 (s), 134 (m), 125 (m), 107 (m).

^{1}H NMR (CD_2Cl_2, δ): 8.95 (s, 12H); 7.04 (s, 3H).

Elemental analysis calculated for $C_{39}H_{15}Cu_3F_{18}N_6$: C 42.58; H 1.37; N 7.64; found: C 42.17; H 1.18; N 7.31.

TGA analysis (1.1134 mg): first weight loss from 187 to 271 °C (−70.63%) corresponds to the loss of 3 molecules of coronene, 1 molecule of copper CTC, and 3 molecules of the starting ligand (via copper CTC decomposition); the second weight loss from 271 °C to 386 °C (−23.40%) corresponds to the loss of a molecule of copper CTC; the third weight loss occurs at 428 °C to 364 °C (−1.5%). The residual weight at 693 °C (5.97%) roughly corresponds to two molecules of CuF_2.

Conclusions

A mechanochemical approach to the preparation of a hybrid D/A material based on Ag(I)/Cu(I) CTCs as acceptors and coronene as the donor was applied in this study. Among the approaches, successful outcomes were achieved by using CH_2Cl_2 or THF-assisted grinding in a mortar. The characterization of the obtained solids was compared with that of the precipitate obtained by solvent-mediated methods, featuring the formation of 1 : 1 molar ratio **1–3** adducts. The formation of these D/A adducts is partially revoked by the dissolution in common organic solvents, indicating that the forces between the donor and the acceptors are rapidly overwhelmed by the interactions with the solvents and by the tendency of coronene to self-associate; on the other hand, the mixing of solution of the CTC and coronene yields to ready precipitation of the adducts. Moreover, SEM analyses underlined that the treatment with the solvent in the LAG method is crucial for the formation of the co-crystals at the interface. The formation of the **1–3** charge transfer adducts is characterised by the charge transfer bands observed in the UV visible spectra, the shifts of the IR bands, and the TGA profiles. Interestingly, contrary to what was observed for similar adducts,[6] the charge transfer interactions in adducts **1–3** fully quench the CTC emissions and decrease that of coronene at room temperature in the solid state. Finally, the direct and indirect band gaps for $\{[3,5\text{-}(CF_3)_2pz]Ag\}_3$@coronene, **1**, were calculated, obtaining values that are lower than those obtained for the starting $\{[3,5\text{-}(CF_3)_2pz]Ag\}_3$ and coronene materials by themselves, in the range typical of semiconductors, contributing to prove the interaction between the coronene and the CTCs in the solid state.

Author contributions

RG conceptualized the work. LL, CM and NS performed the preparation and the characterization studies. RG and LL elaborated on the data. RG and LL wrote the manuscript.

Conflicts of interest

There are no conflicts to declare.

Acknowledgements

References

1 J. Zheng, Z. Lu, K. Wu, G.-H. Ning and D. Li, *Chem. Rev.*, 2020, **120**(17), 9675, DOI: **10.1021/acs.chemrev.0c00011**.

2 R. Galassi, M. A. Rawashdeh-Omary, H. V. R. Dias and M. A. Omary, *Comm. Inorg. Chem.*, 2019, **39**, 287, DOI: **10.1080/02603594.2019.1666371**.

3 S. M. Tekarli, T. R. Cundari and M. A. Omary, *J. Am. Chem. Soc.*, 2008, **130**, 1669, DOI: **10.1021/ja076527u**.

4 R. Galassi, M. M. Ghimire, B. M. Otten, S. Ricci, R. N. McDougald, R. M. Almotawa, D. Alhmoud, J. F. Ivy, A. Rawashdeh, V. N. Nesterov, E. W. Reinheimer, L. M. Daniels, A. Burini and M. A. Omary, *Proc. Natl. Acad. Sci. U. S. A.*, 2017, **114**, E5042–E5051, DOI: **10.1073/pnas.1700890114**.

5 M. A. Rawashdeh-Omary, M. D. Rashdan, S. Dharanipathi, O. Elbjeirami, P. Rameshb and H. V. R. Dias, *Chem. Commun.*, 2011, **47**, 1160, DOI: **10.1039/C0CC03964K**.

6 M. A. Omary, O. Elbjeirami, C. S. P. Gamage, K. M. Sherman and H. V. R. Dias, *Inorg. Chem.*, 2009, **48**, 1784, DOI: **10.1021/ic8021326**.

7 H. R. Dias and C. P. Gamage, *Angew. Chem., Int. Ed.*, 2007, **46**, 2192, DOI: **10.1002/anie.200604585**.

8 M. A. Rawashdeh-Omary, M. A. Omary, J. P. Fackler, R. Galassi, B. R. Pietroni and A. Burini, *J. Am. Chem. Soc.*, 2001, **123**, 9689, DOI: **10.1021/ja016279g**.

9 M. M. Olmstead, F. Jiang, S. Attar and A. L. Balch, *J. Am. Chem. Soc.*, 2001, **123**, 3260, DOI: **10.1021/ja0029533**.

10 N. B. Jayaratna, C. V. Hettiarachchi, M. Yousufuddina and H. V. R. Dias, *New J. Chem.*, 2015, **39**, 5092–5095.

11 A. A. Mohamed, M. A. Rawashdeh-Omary, M. A. Omary and J. P. Fackler Jr., *Dalton Trans.*, 2005, 2597.

12 H. V. R. Dias, H. V. K. Diyabalanage, M. A. Rawashdeh-Omary, M. A. Franzman and M. A. Omary, *J. Am. Chem. Soc.*, 2003, **125**, 12072, DOI: **10.1021/ja036736o**.

13 C. N. Burress, M. I. Bodine, O. Elbjeirami, J. H. Reibenspies, M. A. Omary and F. P. Gabbaï, *Inorg. Chem.*, 2007, **46**, 1388, DOI: **10.1021/ic061998n**.

14 R. N. McDougald Jr., B. Chilukuri, H. Jia, M. R. Perez, H. Rabaâ, X. Wang, V. N. Nesterov, T. R. Cundari, B. E. Gnade and M. A. Omary, *Inorg. Chem.*, 2014, **53**, 7485, DOI: **10.1021/ic500808q**.

15 R. Galassi, S. Ricci, A. Burini, A. Macchioni, L. Rocchigiani, F. Marmottini, S. M. Tekarli, V. N. Nesterov and M. A. Omary, *Inorg. Chem.*, 2013, **52**, 14124, DOI: **10.1021/ic401948p**.

16 A. Burini, R. Bravi, J. P. Fackler Jr., R. Galassi, T. A. Grant, M. A. Omary, B. R. Pietroni and R. J. Staples, *Inorg. Chem.*, 2000, **39**, 3158, DOI: **10.1021/ic991492n**.

17 A. Burini, R. Galassi, B. R. Pietroni, J. P. Fackler Jr. and R. J. Staples, *Chem. Commun.*, 1998, 95.

18 A. A. Mohamed, R. Galassi, F. Papa, A. Burini and J. P. Fackler, *Inorg. Chem.*, 2006, **45**, 7770, DOI: **10.1021/ic060792j**.

19 Z. Lu, A. Burini, R. N. McDougald, S. Ricci, L. Luciani, V. N. Nesterov, A.-M. M. Rawashdeh, M. A. Omary and R. Galassi, *Eur. J. Inorg. Chem.*, 2022, e202101056, DOI: **10.1002/ejic.202101056**.

20 A. Burini, J. P. Fackler, R. Galassi, A. Macchioni, M. A. Omary, M. A. Rawashdeh-Omary, B. R. Pietroni, S. Sabatini and C. Zuccaccia, *J. Am. Chem. Soc.*, 2002, **124**, 4570, DOI: **10.1021/ja0174837**.

21 Q. Li, Y. Zhang, Z. Xie, Y. Zhen, W. Hud and H. Dong, *J. Mater. Chem. C*, 2022, **10**, 2411.

22 J. Mei, Y. Diao, A. L. Appleton, L. Fang and Z. Bao, *J. Am. Chem. Soc.*, 2013, **135**, 6724, DOI: **10.1021/ja400881n**.

23 O. Jurchescu, M. Popinciuc, B. J. van Wees and T. T. M. Palstra, *Adv. Mater.*, 2007, **19**, 688, DOI: **10.1002/adma.200600929**.

24 T. Takahashi, T. Takenobu, J. Takeya and Y. Iwasa, *Appl. Phys. Lett.*, 2006, **88**, 033505, DOI: **10.1063/1.2166698**.

25 G. Giri, E. Verploegen and S. Mannsfeld, *et al.*, *Nature*, 2011, **480**, 504, DOI: **10.1038/nature10683**.

26 G. Hong, X. Gan, C. Leonhardt, Z. Zhang, J. Seibert, J. M. Busch and S. Bräse, *Adv. Mater.*, 2021, **33**, 2005630, DOI: **10.1002/adma.202005630**.

27 Z.-G. Zhang and Y. Li, *Angew. Chem., Int. Ed.*, 2021, **60**, 4422.

28 R. Zhang, H. Zheng and J. Shen, *Synth. Met.*, 1999, **105**, 49, DOI: **10.1016/S0379-6779(99)00056-9**.

29 C. Wang, J. Wang, N. Wu, M. Xu, X. Yang, Y. Lubc and L. Zang, *RSC Adv.*, 2017, **7**, 2382, DOI: **10.1039/C6RA25447K**.

30 J. C. Sorli, P. Friederich, B. Sanchez-Lengeling, N. C. Davy, G. Olivier, N. Ndjawa, H. L. Smith, X. Lin, S. A. Lopez, M. L. Ball, A. Kahn, A. Aspuru-Guzik and Y.-L. Loo, *J. Mater. Chem. C*, 2021, **9**, 1310–1317, DOI: **10.1039/D0TC05092J**.

31 D. Braga, S. L. Giaffreda, F. Grepioni, A. Pettersen, L. Maini, M. Curzi and M. Polito, *Dalton Trans.*, 2006, 1249, DOI: **10.1039/B516165G**.

32 W.-X. Ni, Y.-M. Qiu, M. Li, J. Zheng, R. W.-Y. Sun, S.-Z. Zhan, S. W. Ng and D. Li, *J. Am. Chem. Soc.*, 2014, **136**, 9532, DOI: **10.1021/ja5025113**.

33 H. V. R. Dias, S. A. Polach and Z. Wang, *J. Fluorine Chem.*, 2000, **103**, 163, DOI: **10.1016/S0022-1139(99)00313-9**.

34 M. M. Ghimire, O. C. Simon, L. M. Harris, A. Appiah, R. M. Mitch, V. N. Nesterov, A. Macchioni, C. Zuccaccia, H. Rabaâ, R. Galassi and M. A. Omary, *Inorg. Chem.*, 2019, **58**, 15303, DOI: **10.1021/acs.inorgchem.9b02294**.

35 R. Hahn, F. Bohle, W. Fang, A. Walther, S. Grimme and B. Esser, *J. Am. Chem. Soc.*, 2018, **140**, 17932, DOI: **10.1021/jacs.8b08823**.

36 R. Hahn, F. Bohle, S. Kotte, T. J. Keller, S.-S. Jester, A. Hansen, S. Grimme and B. Esser, *Chem. Sci.*, 2018, **9**, 3477, DOI: **10.1039/C7SC05355J**.

37 A. L. Garay, A. Pichona and S. L. James, *Chem. Soc. Rev.*, 2007, **36**, 846, DOI: **10.1039/B600363J**.

38 A. V. Rask and W. Jones, Crystal Engineering of Organic Cocrystals by the Solid-State Grinding Approach, in *Organic Solid State Reactions. Topics in Current Chemistry*, ed. F. Toda, Springer, Berlin, Heidelberg, 2005, vol. 254, DOI: **10.1007/b100995**.

39 N. Shan, F. Toda and W. Jones, *Chem. Commun.*, 2002, 2372, DOI: **10.1039/B207369M**.

40 Q. Li and Z. Li, *Adv. Sci.*, 2017, **4**, 1600484, DOI: **10.1002/advs.201600484**.

41 Y. Huang, J. Xing and Q. Gong, *et al.*, *Nat. Commun.*, 2019, **10**, 169, DOI: **10.1038/s41467-018-08092-y**.

42 K. Shirai, M. Matsuoka and K. Fukunishi, *Dyes Pigm.*, 1999, **42**, 95, DOI: **10.1016/S0143-7208(99)00013-3**.

43 S. Doose, H. Neuweiler and M. Sauer, *ChemPhysChem*, 2009, **10**, 1389, DOI: **10.1002/cphc.200900238**.

44 P. G. Schroeder, C. B. France, B. A. Parkinson and R. Schlaf, *J. Appl. Phys.*, 2002, **91**, 9095, DOI: **10.1063/1.1473217**.

45 R. B. Sutherland, *Joule*, 2020, **4**, 984, DOI: **10.1016/j.joule.2020.05.001**.

46 O. Akhavan, H. Tohidi and A. Z. Moshfegh, *Thin Solid Films*, 2009, **517**, 6700, DOI: **10.1016/j.tsf.2009.05.016**.